Available online at www.sciencedirect.com
SCIENCE DIRECT®
International Journal of Heat and Fluid Flow 27 (2006) 456–465
International Journal of HEAT AND FLUID FLOW
www.elsevier.com/locate/ijhff

# Lattice-Boltzmann modelling of natural convection in an inclined square enclosure with partitions attached to its cold wall

Ahmed Mezrhab [a], Mohammed Jami [a], Cherifa Abid [b], M'hamed Bouzidi [c], Pierre Lallemand [d,*]

[a] Faculté des Sciences, Département de Physique, Université Mohamed I, Oujda, Morocco
[b] Ecole polytechnique Universitaire de Marseille, IUSTI U.M.R. No 6595, Technopole Château Gombert, 5 Rue Enrico Fermi, 12453 Marseille cedex 13, France
[c] Université Clermont-2, I.U.T. Ave A. Briand, 03100 Montluçon, France
[d] LIMSI, Bâtiment 508, Université Paris-Sud, 91405 Orsay, France

Received 3 August 2004; received in revised form 27 October 2005; accepted 1 November 2005
Available online 10 January 2006

**Abstract**

In the present work, a numerical study of the effect of a single and multiple partitions on heat transfer phenomena in an inclined square cavity, differentially heated, is carried out for $Pr = 0.71$ and Rayleigh numbers of $Ra = 10^3$–$10^6$. The partitions are attached to the cold wall of the cavity. Numerical coupling between the lattice Boltzmann equation and finite-difference for the temperature is used to solve this problem. The investigation is performed for various inclination angles and gap widths $W$. At lower $Ra$ ($Ra \leqslant 10^5$), the average hot wall Nusselt number $Num$ is higher in inclined cavities than in vertical ones; while at larger $Ra$ ($Ra = 10^6$), the opposite occurs. In vertical cavities, $Num$ decreases with decreasing $W$. However in inclined ones, this trend is found only at lower $Ra$ whereas at higher $Ra$, $Num$ shows a maximum at about $W = 0.5$. $Num$ also decreases when the number of partitions ($N_p$) attached to the cold wall of the enclosure increases; however beyond a certain value of ($N_p$), which depends of $Ra$, $Num$ becomes almost constant.


*PACS:* 44.25i.+f; 47.11i.+j

*Keywords:* Lattice-Boltzmann equation; Natural convection; Average Nusselt number; Partitions

## 1. Introduction

Natural convection heat transfer and fluid flow in partitioned enclosures has received considerable attention in recent years because of its modern applications to cooling of printed circuit boards, solar energy collectors, building construction, nuclear engineering, etc. For example, in the study of the solar collectors the determination of the overall heat transfer rates lost towards the ambiant is very important. An excellent review of the past experimental and numerical studies reporting on the flow structures and heat transfer rates in enclosures with partition attached at the top wall and/or at the bottom wall, one extending upwards and the other downwards, can be found in Khan and Yaho (1993). Nansteel and Greif (1984) carried out experimental studies for a rectangular enclosure fitted with a vertical adiabatic partition. The investigations were conducted with water for Rayleigh numbers over the ranges ($10^{10}$–$10^{11}$) and an aspect ratio (height:width ratio) of one-half. They observed the flow separation to occur in front of the divider. For the same problem, experimental and analytical results were also described by Lin and Bejan (1983). Flow patterns similar to those observed by Nansteel and Greif (1984) were

* Corresponding author.
*E-mail addresses:* mezrhab@sciences.univ-oujda.ac.ma (A. Mezrhab), m.jami@sciences.univ-oujda.ac.ma (M. Jami), cherifa.abid@polytech.univ-mrs.fr (C. Abid), bouzidi@asci.fr (M. Bouzidi), lalleman@asci.fr (P. Lallemand).

0142-727X/$ - see front matter © 2005 Published by Elsevier Inc.
doi:10.1016/j.ijheatfluidflow.2005.11.002

**Nomenclature**

| | |
|---|---|
| $A$ | aspect ratio, $(A = H/L)$ |
| $d$ | partition length |
| $g$ | acceleration of gravity |
| $H$ | enclosure height |
| $k$ | thermal conductivity |
| $L$ | enclosure width |
| $N_p$ | number of partitions |
| $Num$ | average hot wall Nusselt number, $\frac{-1}{\Delta T}\int_0^H (\frac{\partial T}{\partial x})_{x=L}\,dy$ |
| $Nu$ | local Nusselt number, $-H(\frac{\partial T}{\partial x})/\Delta T$ |
| $Pr$ | Prandtl number, $(Pr = 0.71)$ |
| $Ra$ | Rayleigh number, $g\beta\Delta T L^3/\nu\alpha_f$ |
| $R_\alpha$ | thermal diffusivity ratio, $\alpha_p/\alpha_f$ |
| $T_c$ | temperature of the cold wall |
| $T_h$ | temperature of the hot wall |
| $T_0$ | average fluid temperature, $(T_h + T_c)/2$ |
| $u$ | dimensional $x$ velocity component |
| $v$ | dimensional $y$ velocity component |
| $w$ | width of the gap connecting the two chambers, Fig. 2 |
| $W$ | dimensionless width of the gap, $W = w/L$ |
| $x$, $y$ | dimensional Cartesian coordinates |
| $X$, $Y$ | dimensionless Cartesian coordinates, $X = x/L$, $Y = y/L$ |

*Greek symbols*

| | |
|---|---|
| $\alpha$ | thermal diffusivity |
| $\beta$ | volumetric expansion coefficient |
| $\delta$ | partition thickness |
| $\delta^*$ | dimensionless partition thickness, $\delta^* = \delta/L$ |
| $\Delta X$, $\Delta Y$ | dimensionless grid spacings in $x$ and $y$ directions |
| $\Delta T$ | maximal difference temperature, $T_h - T_c$ |
| $\theta$ | dimensionless temperature, $\theta = (T - T_0)/\Delta T$ |
| $\nu$ | kinematic viscosity of the fluid |
| $\phi$ | inclination angle |
| $\psi$ | stream function |
| $\Psi$ | dimensionless stream function, $\psi/\alpha_f$ |
| $\Psi_{max}$ | maximum dimensionless stream function |

*Subscripts*

| | |
|---|---|
| f | fluid |
| p | partition |

noted, however the Nusselt numbers obtained were considerably lower than Nansteel and Greif's data. Not so many research works were done on completely partitioned enclosures and most of them were about vertically divided enclosures with very thin partition so that the heat transfer within a partition is essentially one-dimensional (Kelkar and Patankar, 1990; Nakamura and Asko, 1986). Acharya and Jetli (1990) studied numerically the heat transfer and the fluid flow within a square cavity divided by a single obstacle, attached to the ceiling or to the floor. They considered different positions and heights of the partition. They showed that the heat transfer is strongly influenced by the height of the partition; nevertheless, its position has a rather weak effect on the total heat transfer. Mezrhab and Bchir (1999) have investigated numerically the effect of adding a thick partition located vertically close to the hot wall of a differentially heated cavity, forming a narrow vertical channel in which the flow is controlled by vents at the bottom and top of the partition. They have shown that radiation has a significant influence on the flow and heat transfer in the channel. Frederick (1989) has studied numerically natural convection in an air-filled, differentially heated, inclined square cavity, with a single partition attached to its cold wall, at Rayleigh numbers of $10^3$–$10^5$. He showed that the partition leads to convection suppression, and reduces the heat transfer by up to 47% in comparison to the empty cavity at the same Rayleigh number. He has used a finite difference over-relaxation procedure for the solution of the mass, momentum and energy transfer governing equations.

In this paper, we consider the same geometry as that studied by Frederick (1989). We investigate numerically the effect of adding a single or multiple partitions to the cold wall of an air-filled, differentially heated, inclined square cavity, at Rayleigh numbers of $10^3$–$10^6$. This study enables us to determine the influences of gap width and of the number of partitions on the reduction of heat losses from flat plate solar collectors. We propose to use a numerical scheme with coupling between the lattice Boltzmann method for the fluid flow and finite-difference for the temperature. In the lattice-Boltzmann method (Benzi et al., 1992; Qian et al., 1992; d'Humières, 1992; Lallemand and Luo, 2000) one uses a very simple discretization of space: a square lattice with 9 degrees of freedom at each lattice node. The evolution in time is represented by a simple first order explicit scheme. This method will be described in Section 2. In Section 3 we discuss the numeric code used in this study and its application to simulate the natural convection in square cavity differentially heated. The results, discussions and conclusion are presented in the last sections.

## 2. Lattice Boltzmann equation (LBE)

The lattice Boltzmann equation (referred as LBE) allows to simulate various hydrodynamic situations with satisfactory accuracy. It is based on the statistical description of fluids. As in standard CFD techniques quantities under consideration are computed at a limited number of nodes in space and time. However instead of using as primitive variables velocity and pressure (or related quantities)

LBE deals with a number of real quantities that can be physically interpreted as the population of particles that hop during one time step from a space node to one of its neighbours. For the sake of simplicity we consider here a bidimensional model on a square grid with nine quantities per lattice node located at $\hat{\mathbf{e}}_x j + \hat{\mathbf{e}}_y k$ ($j,k$ integers) where $\hat{\mathbf{e}}_x$ and $\hat{\mathbf{e}}_y$ are vectors of length $l$. If $\tau$ is the time increment then we define nine velocities ($\mathbf{c}_i$, $i = 0,\ldots,8$) of amplitudes 0, $l/\tau$ and $\sqrt{2}l/\tau$ that correspond to no motion, motion to the nearest neighbour and motion to the next nearest neighbour. We note $f_i(j,k)$ nine quantities that are used for the description of the fluid and write in vector form

$$F(\mathbf{r},t) = \{f_0(\mathbf{r},t),\ldots,f_8(\mathbf{r},t)\}^{\mathrm{T}} \tag{1}$$

The dynamics of the system is obtained with a simple first order equation, the so-called LBE,

$$f_i(\mathbf{r}+\mathbf{c}_i, t+\tau) - f_i(\mathbf{r},t) = \Omega F(\mathbf{r},t) \tag{2}$$

The left-hand side can be interpreted as the advection, whereas the right-hand side where $\Omega$ is an operator that acts locally represents the redistribution of particles due to collisions. Note that in the presence of body force, as will be the case here for natural convection, the collision operator includes a "molecular" part and an "interaction" part proportional to that body force.[1]

This dynamic system has been analyzed and tested in numerous situations (Higuera and Jimenez, 1989; Higuera et al., 1989; Benzi et al., 1992; Qian et al., 1992). With proper choice of the collision operator it can be shown that the behaviour of the system at large scale (compared to $l$) and long times (compared to $\tau$) is the same as that of a weakly compressible fluid. It is characterized by transport coefficients that can be expressed with $l$ and $\tau$ and thus one can define non-dimensional numbers like Reynolds, Prandtl or Mach numbers.

Although the dynamical equation (2) is first order in time the overall accuracy is of second order.

It leads to an explicit numerical scheme of local character which allows to use parallel computing without much difficulty. In addition boundary conditions are quite easy to implement starting from the simple "bounce-back" of particles on boundaries as depicted in Fig. 1 when solid boundaries are chosen parallel to the axis $O_x$ of or $O_y$ and located between two lattice nodes. For boundaries of arbitrary shape variants (not much more complicated to implement) of the "bounce-back" scheme have been shown to give quite satisfactory results. See among other propositions Noble et al. (1995), Ginzbourg and d'Humières (1995), Bouzidi et al. (2001), Ginzburg and d'Humières (2003).

For the purpose of the present work, we indicate that we use the more sophisticated form of $\Omega$ following d'Humières (1992). In addition as we shall work in situations where fluid velocities are small so that we shall neglect variations of the density. Under such conditions the fluid velocity $\{u,v\}$ used in the advection–diffusion equation for the temperature is given by

$$u = \sum_i \mathbf{c}_{ix} f_i, \quad v = \sum_i \mathbf{c}_{iy} f_i \tag{3}$$

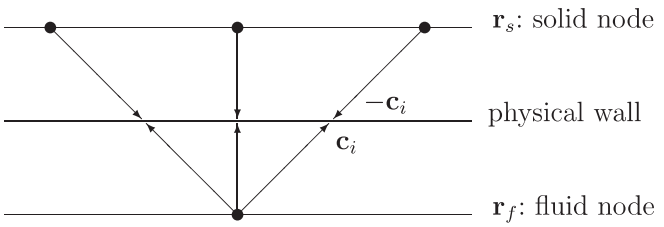


Fig. 1. Bounce-back boundary condition: the $f_i$ going towards the wall goes into $f_i$ with $\mathbf{c}_i = -\mathbf{c}_i$.

## 3. Numerical procedure

The numerical procedure used is based on the Boltzmann method to simulate the flow and the finite-difference method for the resolution of the energy equation. This procedure gives very good results in the simulation of the convective flows as it was shown by Mezrhab et al. (2004). As a matter of fact, many attempts have been made to simulate the thermal effects with LBE techniques (Alexander et al., 1993). However, this path presented difficulties as far as isotropy and stability (Pavlo et al., 1998; Lallemand and Luo, 2003) are concerned. Then, it is more convenient to treat separately density and momentum (athermal fluid) and temperature. In our case, the coupling between the flow and the temperature field is done as follows: Temperature $T$ provides a buoyancy force in the $x$ and $y$ directions because the square cavity is inclined by an angle $\phi$ with respect to the horizontal. Therefore, as indicated after Eq. (2), we increment the $x$ and $y$ components of the linear momentum respectively by $f_x = -g\beta(T(\mathbf{r},t) - T_0)\cos\phi$ and $f_y = g\beta(T(\mathbf{r},t) - T_0)\sin\phi$ where $\mathbf{r}$ is the position of the air node which has temperature $T(\mathbf{r},t)$ at time $t$. The usual LBE analysis of the long time, large spatial scale behaviour leads to "Navier–Stokes"-like equations with the adequate coupling between the temperature field and the hydrodynamical variables, and unmodified expressions for the viscosity. The energy equation is discretized by the finite-difference method (with a fourth order stencil for space derivatives) and provides us the temperature field inside the cavity.

$$\frac{\partial T}{\partial t} + u\frac{\partial T}{\partial x} + v\frac{\partial T}{\partial y} = R_\alpha \alpha_{\mathrm{f}}\left(\frac{\partial^2 T}{\partial x^2} + \frac{\partial^2 T}{\partial y^2}\right) \tag{4}$$

where $R_\alpha = 1$ in the fluid region and $R_\alpha = \alpha_{\mathrm{p}}/\alpha_{\mathrm{f}}$ in the solid region. $u$ and $v$ are obtained from the LBE system. Let us note that the terms introduced to couple flow and temperature neglect compressibility. We consider a square cavity

[1] Following the point of view of moments, see for instance (Lallemand and Luo, 2000), the "interaction" part acts to modify the components of the linear momentum, which otherwise are not affected by the "molecular" part of $\Omega$.

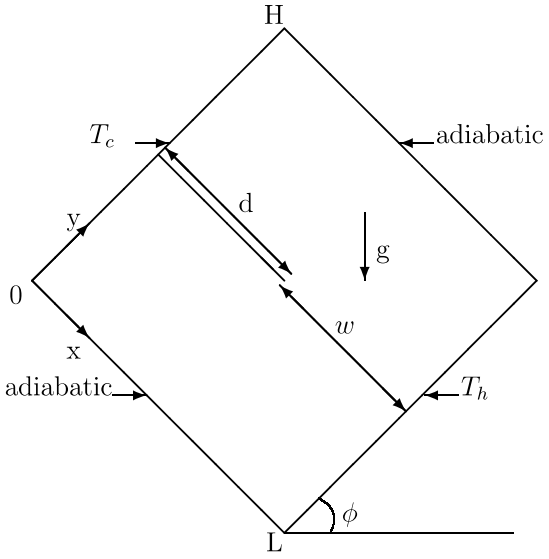


Fig. 2. Square cavity simulated.

with two walls maintained respectively at $T_c$ and $T_h$, making an angle $\phi$ with the horizontal. The other two walls are adiabatic, midway between them, and parallel to them, a partition of length $d$ and thickness $\delta$ is fitted to the cold wall as indicated in Fig. 2. $w$ is the width of the gap where the fluid flows. In the present paper, natural convection in a divided square cavity is simulated by using the coupling between the LBE and finite-difference. If the grid of LBE nodes has size $N_x \times N_y = N^2$ for $N_x = N_y = N$, according to the bounce-back boundary condition and LBE techniques, the effective boundaries will be at 1/2 and $N + 1/2$. We may use for the finite-difference scheme the same grid nodes as for the LBE scheme. In that case, we must therefore use as boundary conditions for the temperature.

$$T(1/2, y) = T_c \quad \text{for } \frac{1}{2} \leqslant y \leqslant N + \frac{1}{2}$$

$$T(N + 1/2, y) = T_h \quad \text{for } \frac{1}{2} \leqslant y \leqslant N + \frac{1}{2}$$

$$\frac{\partial T}{\partial y}(x, 1/2) = 0 \quad \text{for } \frac{1}{2} \leqslant x \leqslant N + \frac{1}{2}$$

$$\frac{\partial T}{\partial y}(x, N + 1/2) = 0 \quad \text{for } \frac{1}{2} \leqslant x \leqslant N + \frac{1}{2}$$

On the enclosure walls and the partition $u = v = 0$. The partition should be very thin ($d \gg \delta$), and transparent to solar radiation, in order not to interfere with solar energy collection.

## 4. Sensitivity to the grid size

The mathematical model developed in the previous section was used to investigate the natural convection in a divided cavity. We first varied the grid to determine the optimum uniform grid (i.e. the best compromise between accuracy and computational costs). Fig. 3(a) and (b) illustrate the grid dependence of the solution for an enclosure

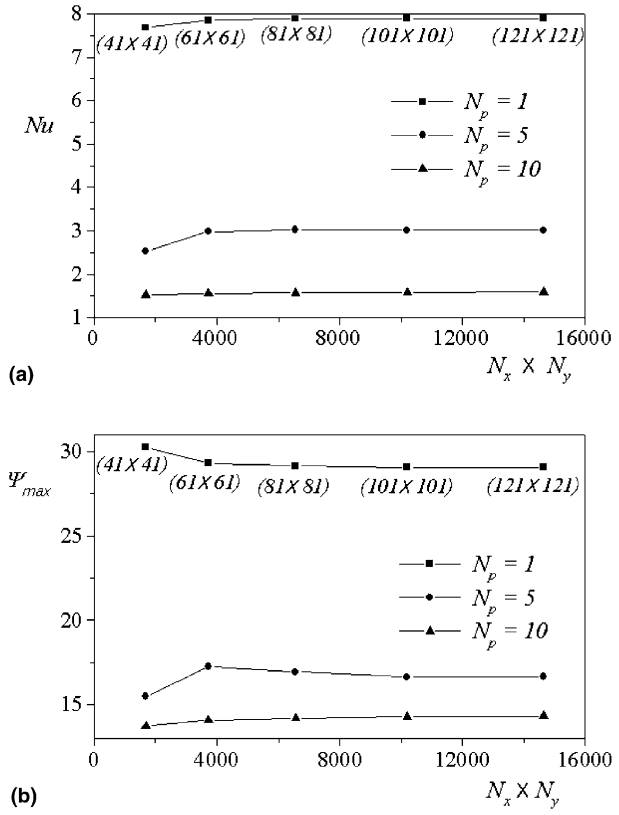


Fig. 3. The influence of mesh size on the accuracy of the results for $Ra = 10^6$, $\phi = 45°$, $W = 0.5$: (a) the average hot wall Nusselt number, (b) the maximum stream function.

divided by one partition of length $d = 0.5 \times L$ (i.e. $W = 0.5$). The average hot wall Nusselt number (a) and the maximum of the stream function (b) are reported against the mesh size $N_x \times N_y = N^2$. One estimates that the solution becomes grid independent at $N_x \times N_y = 81 \times 81$ for $N_p = 1$ and at $N_x \times N_y = 101 \times 101$ for $N_p = 10$. Consequently, for the computations reported in this study a grid with $81 \times 81$ points was chosen for the cavity with only one partition case and $101 \times 101$ for the cavity with multiple partitions to optimize the relation between accuracy and computing time.

## 5. Code validation

The code was extensively used on benchmark problems to check its validity. In the cases of an empty cavity, a square cavity with a hot circle inside, and concentric cylinders, the presented numerical study was checked for accuracy against the earlier published numerical and experimental results reported by different authors, and the agreement between the present and previous results was very good in Mezrhab et al. (2004). For this reason, it is not repeated here for brevity. In this paper, we have chosen to present the code validation for two kinds of cavities divided by a thin partition. First, calculations were performed for the configuration studied by Kelkar and Patankar (1990) who have modelled natural convection by the

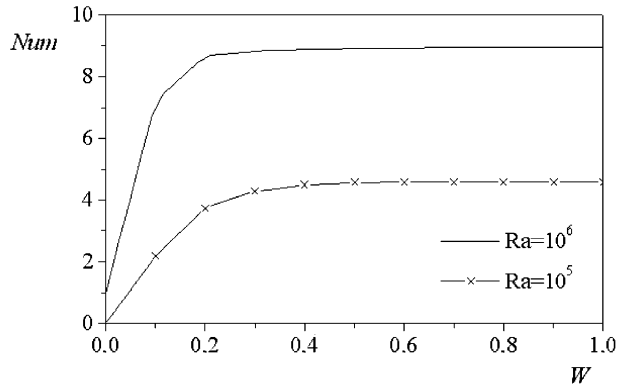


Fig. 4. Variation of the average Nusselt number with gap width for a perfectly insulated partition.

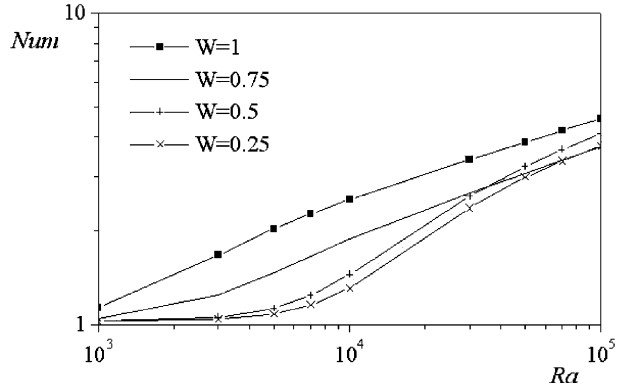


Fig. 5. Variation of the average Nusselt number with $Ra$ and $W$ for $\phi = 45°$.

finite-difference method in a square cavity with a single partition located vertically at the center of the enclosure. As example of this validation, we present in Fig. 4 the variation of the average Nusselt number with dimensionless width of the gap connecting the two chambers of the cavity for two Rayleigh numbers and a perfectly insulating partition. We notice that Fig. 4 can be favourably graphically compared with Fig. 2(a) presented in Kelkar and Patankar (1990). Second, results were validated with those reported by Frederick (1989) who used the finite-difference method to simulate natural convection in a similar configuration to the one considered in this paper. Fig. 5 shows the variation of the average Nusselt number with the Rayleigh number for a cavity inclined by 45° with respect to the horizontal and for various partition lengths. There also, an excellent agreement is noted between results presented in Fig. 5 and those displayed in Fig. 4(b) of Frederick (1989). Despite the fact that no numerical data which were reported in (Kelkar and Patankar, 1990; Frederick, 1989), the largest discrepancies between the present results and those graphically shown in (Kelkar and Patankar, 1990; Frederick, 1989) can be estimated to be less than 2%.

Based on the above studies, it was concluded that our code could be reliably applied to the problem considered here.

## 6. Results and discussion

Each case required the specification of seven dimensionless parameters ($Pr, R_\alpha, A, Ra, N_p, W, \delta^*$) among which the Prandtl number, the thermal diffusivity ratio, the cavity aspect ratio and the dimensionless partition thickness were held fixed respectively at $Pr = 0.71$, $R_\alpha = 1$, $A = 1$ and $\delta^* = \Delta Y$. The ranges covered by the remaining parameters were $10^3 \leqslant Ra \leqslant 10^6$, $0 \leqslant N_p \leqslant 10$ and $0.25 \leqslant W \leqslant 1$. The isotherms are plotted using the dimensionless temperature $\theta$. When the Rayleigh number exceeds $10^6$, the solution becomes time dependent. The transition to time dependence of the solution depends upon the angle $\phi$ and the partition length $d$. For example, we found that for a square cavity inclined by an angle $\phi = 45°$ divided by one partition of length $d = 0.5 \times L$, transition to time dependence takes place between $Ra = 2 \times 10^6$ and $Ra = 3 \times 10^6$.

### 6.1. Cavity with only one partition

For an angle $\phi = 90°$ and $W = 0.5$, we present the streamlines and isotherms at $Ra = 10^4$, $Ra = 10^5$ and $Ra = 10^6$ in Figs. 6–8 respectively. Let us note that the streamlines circulate counter-clockwise owing to the

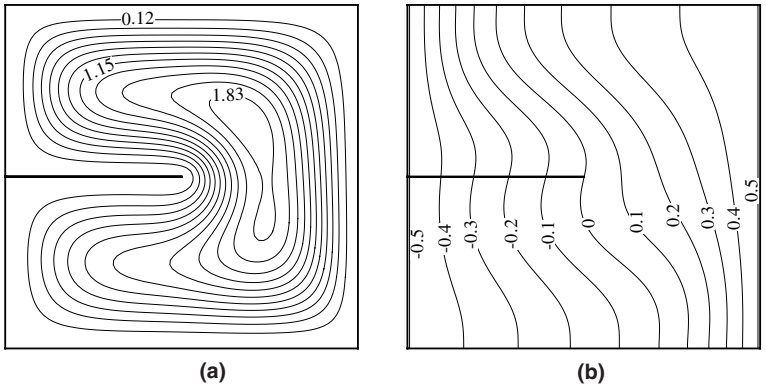


Fig. 6. Isograms at $Ra = 10^4$, $W = 0.5$, $\phi = 90°$: (a) streamlines; (b) isotherms.

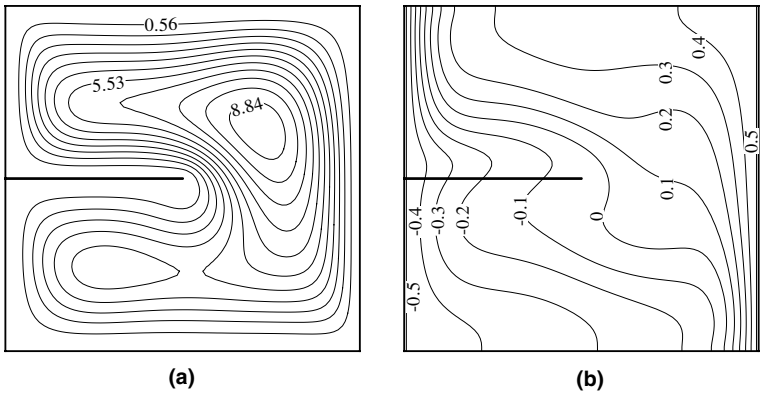


Fig. 7. Isograms at $Ra = 10^5$, $W = 0.5$, $\phi = 90°$: (a) streamlines; (b) isotherms.

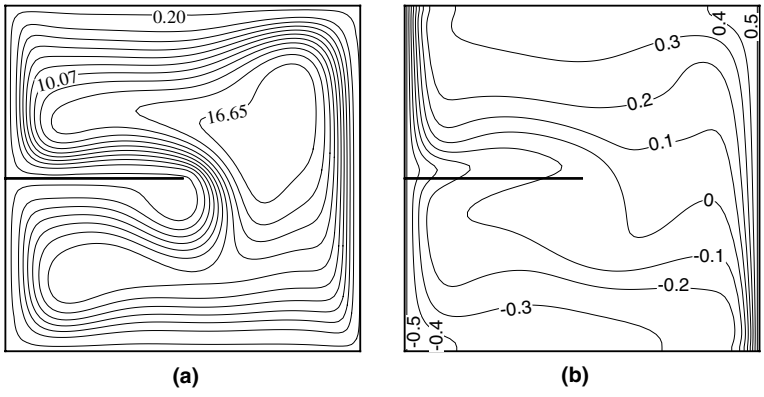


Fig. 8. Isograms at $Ra = 10^6$, $W = 0.5$, $\phi = 90°$: (a) streamlines; (b) isotherms.

positions of the cold and hot walls. However, it is clear that they are not symmetric with respect to the center of the cavity as what can be observed in the case of an empty cavity. The point of maximum stream function, which is located at the centre of the empty cavity, is displaced upwards and towards the hot part of the cavity. It is also noted that the increase of *Ra* provokes an increase in the air velocity. This is due to the buoyancy force which becomes important at high Rayleigh numbers. The increase of the air velocity is more pronounced close to the hot wall, the upper part of the cold wall and the upper surface of the partition. As a matter of fact, in these regions the air flow is not very affected by the presence of the partition; whereas in the other parts of the cavity the air velocity is reduced by the partition. The isotherms are shown in Figs. 6(b), 7(b) and 8(b). In the case of the empty square cavity, at $Ra = 10^4$, the isotherms are nearly horizontal and this mode of flow is characterized by a vertical gradient of temperature. The flows ascending and downward are contiguous, the flow being unicellular. However, in presence of the partition, the isotherms become nearly vertical, especially around the partition. This behavior is observed also at higher Rayleigh numbers, although as *Ra* increases, the boundary layers and the temperature stratification tend to reappear, especially in the upper and lower parts of the cavity. The partition modifies much the temperature fields. The isotherms show that heat flow through the partition is upwards. At $Ra = 10^6$, up and below the partition, the isotherms tend to become horizontal as in the case of the empty cavity. Significant horizontal temperature gradients are established at different levels of the vertical midplane.

Fig. 9(a) shows the variation of the average hot wall Nusselt number *Num* according to *Ra* and *W* at $\phi = 90°$. Independently of the value of *W*, *Num* increases with increasing *Ra*. This is due to the increase of the buoyancy force. On the other hand, for a fixed value of *Ra*, *Num* increases with increasing *W*. However, this increase is especially pronounced in the range of Rayleigh numbers $3 \times 10^3$–$2 \times 10^4$. In fact, when *Ra* is lower ($Ra \leqslant 10^3$), the conduction heat transfer is the predominant mode. Hence, the effect of *W*, on the average hot wall Nusselt number, is negligible since the thermal conductivity of the partition is the same of that of the air. When $3 \times 10^3 \leqslant Ra \leqslant 2 \times 10^4$, heat transfer by natural convection and conduction are of the same magnitude (mode of transition). So, the partition prevents the fluid motion in the enclosure and its obstacle effect is more important when its length is greater (small *W*). However, when $Ra > 2 \times 10^4$, the boundary layers formed on all solid walls become progressively thinner owing to the buoyancy force which is large. Thus, heat transfer is essentially dominated by natural convection; which

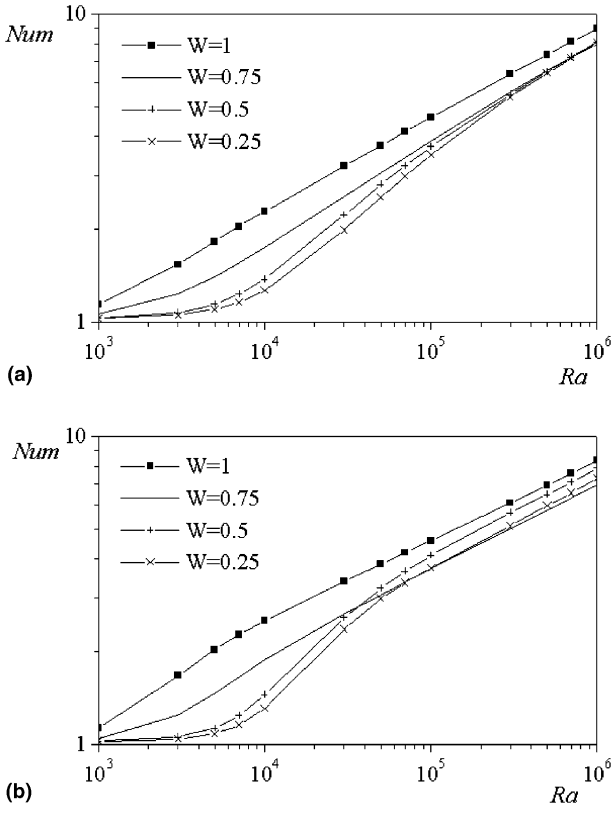


Fig. 9. Variation of the average hot wall Nusselt number with $Ra$ and $W$: (a) $\phi = 90°$; (b) $\phi = 45°$.

explains that isotherms and streamlines (Fig. 8) near the hot wall tend to resemble those observed in the empty cavity. Therefore, at high Rayleigh number the role of the partition length is less important and the average hot wall Nusselt number is practically the same for the three values of $W$.

To present the results in the case of an inclined cavity, we take $\phi = 45°$. Fig. 9(b) shows the variation of the average hot wall Nusselt number as a function of $Ra$ and $W$. The average hot wall Nusselt number decreases with decreasing $W$ until a Rayleigh number equal to $4 \times 10^4$. Beyond this value of $Ra$, $Num$ obtained for $W = 0.5$ exceeds the one corresponding to $W = 0.75$. In the same way, one notices that $Num$ ($W = 0.25$) becomes higher than $Num$ ($W = 0.75$) when $Ra$ exceeds $2 \times 10^5$. These occurrences are maintained as $Ra$ increases. As a matter of fact, when $Ra$ is lower ($Ra \cong 10^4$), the buoyancy force is weak and the fluid flow in the cavity is not strong. Thus, this motion of air becomes even weaker when the length of the partition is large. This can be seen, in Figs. 11(a), 12(a) and 13(a), showing that the maximum dimensionless stream function $\Psi_{\max}$ is increased from 1.46 to 4.68 when the partition length is decreased from 0.75 to 0.25. In addition, the local Nusselt number, as shown in Fig. 10, is higher for $W = 0.75$ than for other gap widths along most of the hot wall (until $Y = 0.7$). The local Nusselt number obtained for $W = 0.25$ is the smallest, except in the top part of the hot wall defined by ($Y \geqslant 0.6$). However, at high Rayleigh numbers ($Ra = 10^6$), the variation of $Num$ with $Ra$ and $W$ is more

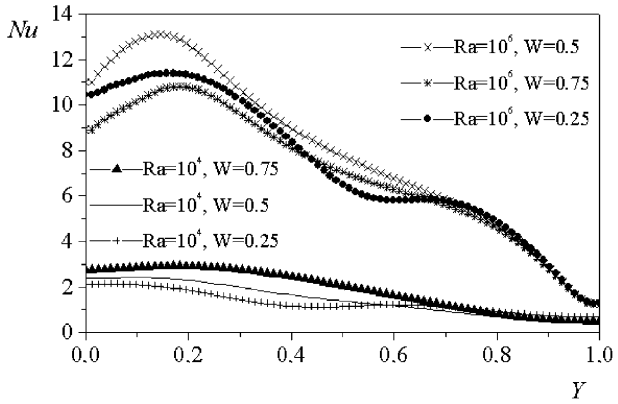


Fig. 10. Local Nusselt number on hot wall, $\phi = 45°$.

complex. It can be explained by the evolution of the local Nusselt number along the hot wall. At $W = 0.5$ and 0.75, the local Nusselt number (Fig. 10) has only one maximum close to the bottom part of the hot wall; whereas at $W = 0.25$, two local maxima are observed in the local Nusselt number. This is because at $W = 0.25$, a second vortex appears in the lower half of the cavity and a transition to bicellular flow occurs (Fig. 11(b)). In fact, the part of the fluid cooled by the cold wall is diverted by the partition towards the hot one, producing a local increase in $Nu$ from $Y = 0.5$ upwards. The local Nusselt number for $W = 0.5$ is the greatest along the most part of the hot wall (until $Y = 0.7$). This is because of the thinning of the boundary layers near the lower part of the cold wall as shown in Fig. 12(b). Therefore, in this region, the air velocity is strong and it allows it to be cooled more effectively by the cold wall. Hence, the increase in the local Nusselt number. For $W = 0.25$, the local Nusselt number along the hot wall presents a minimum between $Y = 0.4$ and $Y = 0.7$ (Fig. 10). Indeed, the partition diverts the air cooled, ascending and descending, respectively towards the cold and hot wall. This creates a region located between $Y = 0.4$ and $Y = 0.7$ where the boundary layers are thick (Fig. 11(b)) and consequently the local Nusselt number is weak. Finally, for $W = 0.75$, a secondary flow which circulates in the clockwise direction, appears in the lower left quarter of the cavity (Fig. 13(b)). This flow disturbs the circulation and the portion of air, cooled by the bottom part of the cold wall, is reduced. Consequently, the air circulating close to the lower part of the hot wall is less cooled, which explains the low value of the local Nusselt number in this region.

Figs. 11–13 show the effect of the partition length on streamlines in an inclined cavity for two values of $Ra$. It is evident for $Ra = 10^4$ that an increase in partition length increases the asymmetry of the flow pattern and decreases the dimensionless stream function, therefore the circulation and the heat transfer decreases in the cavity (Fig. 9(b)). At $Ra = 10^6$, this behavior is considerably modified and some vortex regions appear. The circulation of the fluid in the cavity is made in a thin layer adjacent to the bounding walls and around the partition. At high $Ra$, the heat trans-

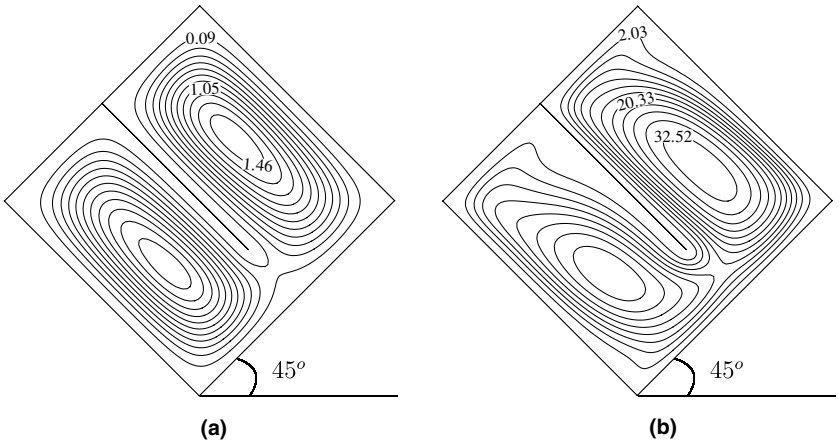


Fig. 11. Streamlines at $\phi = 45°$, $W = 0.25$: (a) $Ra = 10^4$; (b) $Ra = 10^6$.

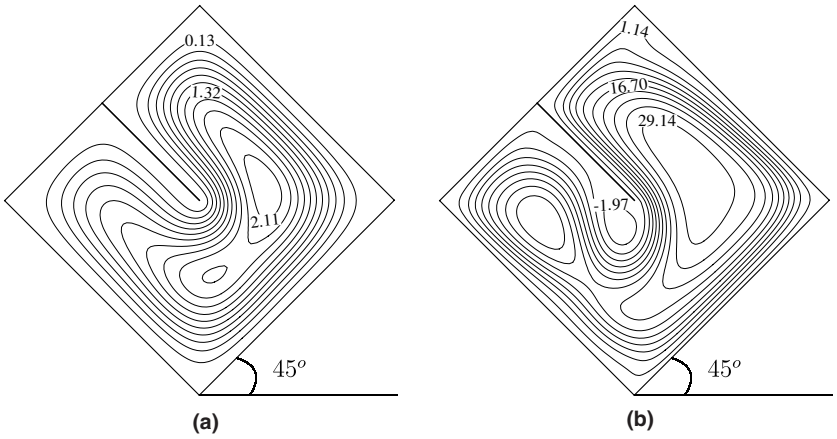


Fig. 12. Streamlines at $\phi = 45°$, $W = 0.5$: (a) $Ra = 10^4$; (b) $Ra = 10^6$.

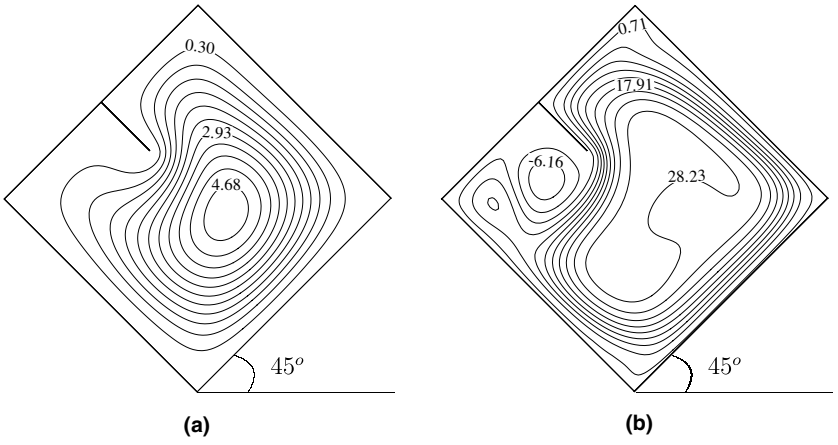


Fig. 13. Streamlines at $\phi = 45°$, $W = 0.75$: (a) $Ra = 10^4$; (b) $Ra = 10^6$.

fer reduction is affected by a secondary buoyancy force generated by the partition. When the partition length decreases, the flow separates below the partition although at $W = 0.25$, a noticeable separation bubble is not predicted. The size and strength of the recirculation bubble increase as the partition length decreases.

The effects of the main parameters on the average hot wall Nusselt number are summarized, in Fig. 14, as follows: at lower values of $Ra$ ($Ra \leqslant 10^5$), the average hot wall Nusselt number is higher in inclined cavities than in vertical ones; whereas at higher values of $Ra$ ($Ra = 10^6$), the opposite situation occurs. At lower Rayleigh numbers,

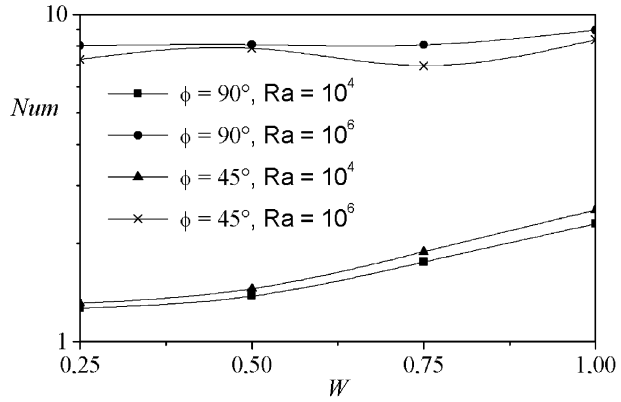


Fig. 14. Variation of the average hot wall Nusselt number with $W$.

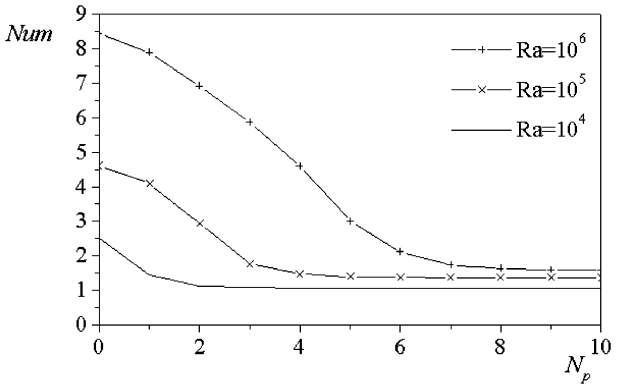


Fig. 16. Variation of the average hot wall Nusselt number with number of partitions for various $Ra$.

the average hot wall Nusselt number decreases with the decrease of the gap width whatever the inclination angle of the cavity. The same tendency is observed at higher $Ra$ only in vertical cavities. At $Ra = 10^6$ and in the case of a divided cavity inclined by an angle $\phi = 45°$, the average hot wall Nusselt number shows a maximum for $W = 0.5$ and a minimum for $W = 0.75$. The value $W = 0.5$ of the opening width (partition length $d = 0.5 \times L$) will be more interesting than the other values of $W$ such as $W = 0.75$ or 0.25 to reduce the heat transfer. Furthermore, at $W = 0.75$, the heat transfer reduction is nearly constant in the range of $Ra$ from $3 \times 10^3$ to $10^6$; while for the other values of $W$ the heat transfer reduction decreases as $Ra$ increases. In fact, as can be seen in Fig. 9(b), in this range of $Ra$, the curve $Num(Ra)$ remains nearly parallel to that for the empty cavity.

### 6.2. Cavity with multiple partitions

The aim is now to study the effect of multiple partitions attached to the cold wall of the cavity on the heat transfer reduction. It has been hoped to inhibit the natural convection by subdividing the cavity into a number of smaller cells and hence achieve a lower heat transfer rate between the hot and cold walls. We remain in the setting of the physical problem seen early. In this case $\phi = 45°$ and the gap width $W = 0.5$ are taken for all partitions.

Fig. 15 shows the streamlines for $N_p = 2$ and 10. It is shown that the air flow is strongly affected as $N_p$ increases. There will be less air, which can reach the cold wall when the number of partitions is large. The flow being unicellular in the right part of the cavity at higher value of $N_p$. This behavior causes a significant reduction in the heat transfer, as that can be shown in Fig. 16, which gives the variation of the average hot wall Nusselt number with number of partitions ($N_p$).

For every $Ra$ one notices that $Num$ decreases with increasing $N_p$ until a value beyond which $Num$ remains almost constant. Natural convection is reduced when $N_p$ increases until a certain number of partitions is reached for which this exchange mechanism is nearly completely eliminated. At $Ra = 10^6$, the buoyancy force is large. It causes a stronger circulation, and thus more heat is transferred between the hot and cold walls. It is clearly shown that $Num$ has a relatively higher value, for $N_p = 0$, and decreases less rapidly until it becomes nearly constant when $N_p$ exceeds 6. When $Ra$ decreases, $Num$ decreases rapidly with $N_p$, in comparison to the case of $Ra = 10^6$. $Num$

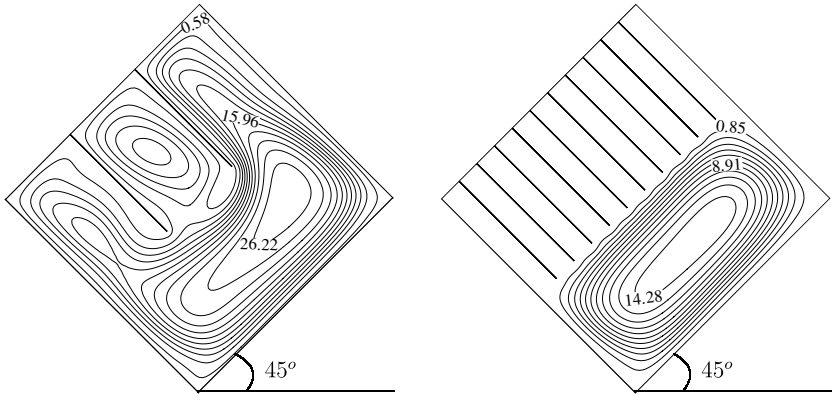


2 Partitions 10 Partitions

Fig. 15. Effect of partitions number on streamlines at $Ra = 10^6$, $\phi = 45°$ and $W = 0.5$.

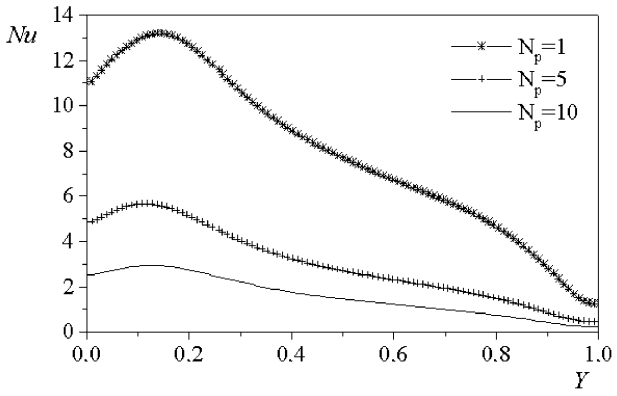


Fig. 17. Variation of the local Nusselt number on the hot wall with number of partitions at $Ra = 10^6$.

becomes almost constant when $N_p$ exceeds 2 for $Ra = 10^4$ and 3 ($Ra = 10^5$). Fig. 17 shows the variation of local Nusselt number on the hot wall, at $Ra = 10^6$, for different numbers of partitions. One notices that $Nu$ decreases when $N_p$ increases. This is because, the air circulation becomes weaker especially near the cold wall. Thus, the air circulating in the neighbourhood of the hot wall is less cooled, which causes an increase in the local Nusselt number.

## 7. Conclusion

A numerical study (coupling LBE/finite-difference) of natural convection in a square cavity, with a single and multiple partitions on its cold wall, has been carried out. The aim of this study was to find a mean to reduce the overall heat transfer rates lost by the solar collectors towards the ambiance. The results show a maximum reduction of the heat transfer between $Ra = 6 \times 10^3$ and $Ra = 2 \times 10^4$ when the cavity is divided by one diathermal partition. Beyond this last value, the reduction decreases progressively. The effect of the partition on the temperature field is marginal at low $Ra$, and grows at higher $Ra$ because in the first case, the boundary layers are thicker and the fluid motion is not prevented as in the last case where the boundary layers are thinner. The heat transfer reduction increases with decreasing $W$ for any value of $Ra$ when the cavity is vertical; however this behavior is valid for an inclined cavity just for small values of $Ra$. In an inclined cavity, at higher value of $Ra$, the heat transfer shows a maximum for $W = 0.5$. The heat transfer reduction is important when the partition length is small ($W = 0.75$). This is due to the flow that separates below the partition although at $W = 0.25$, a noticeable separation bubble is not produced. The size and strength of the recirculation bubble increase as the partition length decreases.

In the case of multiple partitions, the heat transfer reduction is considerably increased when the number of partitions $N_p$ increases until a certain value of $N_p$ for which this reduction remains constant as convection was suppressed.

## References

Acharya, S., Jetli, R., 1990. Heat transfer due to buoyancy in a partially divided square box. Int. J. Heat Mass Transfer 33 (5), 931–942.

Alexander, F.J., Chen, S., Sterling, J.D., 1993. Lattice Boltzmann thermodynamics. Phys. Rev. E 47, R2249–R2252.

Benzi, R., Succi, S., Vergassola, M., 1992. The lattice Boltzmann equation: theory and applications. Phys. Rep. 222, 145–197.

Bouzidi, M., Firdaouss, M., Lallemand, P., 2001. Momentum transfer of a Boltzmann-lattice fluid with boundaries. Phys. Fluids 13, 3452–3459.

d'Humières, D., 1992. Generalized lattice-Boltzmann equations. In: Shizgal, B.D., Weaver, D.P. (Eds.), Rarefied Gas Dynamics: Theory and Simulations, Progress in Astronautics and Aeronautics, vol. 159. AIAA, Washington, DC, pp. 450–458.

Frederick, R.L., 1989. Natural convection in an inclined square enclosure with a partition attached to its cold wall. Int J. Heat Mass Transfer 32, 87–94.

Ginzbourg, I., d'Humières, D., 1995. Second order boundary method for lattice Boltzmann model. J. Stat. Phys. 84, 927–971.

Ginzburg, I., d'Humières, D., 2003. Multi-reflection boundary conditions for lattice Boltzmann models. Phys. Rev. E 68, 066614-1–066614-30.

Higuera, F., Jimenez, J., 1989. Boltzmann approach to lattice gas simulations. Europhys. Lett. 9, 663–668.

Higuera, F., Succi, S., Benzi, R., 1989. Lattice gas dynamic with enhanced collisions. Europhys. Lett. 9, 345–349.

Kelkar, K.M., Patankar, S.V., 1990. Numerical prediction of natural convection in square partitioned enclosure. Numerical Heat Transfer Part A 17, 269–285.

Khan, J.A., Yaho, G.F., 1993. Comparison of natural convection of water and air in a partitioned rectangular enclosure. Int. J. Heat Mass Transfer 36 (12), 3107–3117.

Lallemand, P., Luo, L.S., 2000. Theory of the lattice Boltzmann method: dispersion, dissipation, isotropy, galilean invariance and stability. Phys. Rev. E 61, 6546–6562.

Lallemand, P., Luo, L.-S., 2003. Theory of the lattice Boltzmann method: acoustic and thermal properties in two and three dimensions. Phys. Rev. E 68, 036706-1–036706-25.

Lin, N.N., Bejan, A., 1983. Natural convection in a partially divided enclosure. Int. J. Heat Mass Transfer 26, 1867–1878.

Mezrhab, A., Bchir, L., 1999. Radiation–natural convection interactions in partitioned cavities. Int. J. Numer. Meth. Heat Fluid Flow 9 (2), 186–203.

Mezrhab, A., Bouzidi, M., Lallemand, P., 2004. Hybrid lattice Boltzmann finite-difference simulation of convective flows. Comput. Fluids 33, 623–641.

Nakamura, H., Asko, Y., 1986. Combined free convection and radiation heat transfer in rectangular cavities with a partition wall. Heat Transfer Jpn. Res., 60–81.

Nansteel, M.W., Greif, R., 1984. An investigation of natural convection in enclosures with two- and three-dimensional partitions. Int. J. Heat Mass Transfer 27 (4), 561–571.

Noble, D.R., Chen, S., Georgiadis, J.G., Buckius, R.O., 1995. A consistent hydrodynamic boundary condition for the lattice Boltzmann method. Phys. Fluids 7, 203–209.

Pavlo, P., Vahala, G., Vahala, L., Soe, M., 1998. Linear stability analysis of thermo-lattice Boltzmann models. J. Comput. Phys. 139, 79–91.

Qian, Y.H., d'Humières, D., Lallemand, P., 1992. Lattice BGK models for Navier–Stokes equation. Europhys. Lett. 17, 479–484.